




Publication Year	2023
Acceptance in OA	2024-12-23T12:47:42Z
Title	Jets in FR0 radio galaxies
Authors	GIOVANNINI, Gabriele, BALDI, Ranieri Diego, CAPETTI, Alessandro, GIROLETTI, Marcello, Lico, R.
Publisher's version (DOI)	10.1051/0004-6361/202245395
Handle	http://hdl.handle.net/20.500.12386/35567
Journal	ASTRONOMY & ASTROPHYSICS
Volume	672

Jets in FR0 radio galaxies[★]

G. Giovannini^{1,2} , R. D. Baldi¹, A. Capetti³, M. Giroletti¹, and R. Lico^{4,1}

¹ INAF – Istituto di Radioastronomia, via Gobetti 101, 40129 Bologna, Italy
e-mail: ggiovann@ira.inaf.it

² Dipartimento di Fisica e Astronomia – University of Bologna, via Gobetti 93/2, Italy

³ INAF – Osservatorio Astronomico di Torino, via Osservatorio 2, 10025, Pino Torinese, Italy

⁴ Instituto de Astrofísica de Andalucía-CSIC, Glorieta de la Astronomía s/n, 18008 Granada, Spain

Received 7 November 2022 / Accepted 7 February 2023

ABSTRACT

Context. The local radio-loud AGN population is dominated by compact sources named FR0s. These sources show features, for example the host type, the mass of the supermassive black hole (SMBH), and the multi-band nuclear characteristics, that are similar to those of FRI radio galaxies. However, in the radio band, while FR0 and FRI share the same nuclear properties, the kiloparsec-scale diffuse component dominant in FRI is missing in FR0s. Previous very-long-baseline interferometry (VLBI) observations of a small sample of FR0s show a complex structure, mostly symmetric (two-sided jets) with respect to the central core.

Aims. With this project we would like to study the parsec-scale structure in FR0s in comparison with that of FRI sources. Jets in FRI are relativistic on the parsec scale and decrease their velocity becoming subrelativistic on the kiloparsec scale. We would like to test whether this result also applies to the jets in FR0s or, alternatively, whether they are subrelativistic on the parsec scale. This might be the reason why they are unable to grow, because of instabilities, related to a low jet bulk velocity.

Methods. To this end we observed 18 FR0 galaxies with the VLBA at 1.5 and 5 GHz and/or with the EVN at 1.7 GHz and produced detailed images at milliarcsec resolution of their nuclear emission to study the jet and core structure.

Results. All sources have been detected but one. Four sources are unresolved, even in these high-resolution images; jets have been detected in all other sources. We derived the distribution of the jet-to-counter-jet ratio of FR0s and found that it is significantly different from that of FRIs, suggesting different jet bulk speed velocities.

Conclusions. Combining the present data with published data of FR0 with VLBI observations, we derive that the radio structure of FR0 galaxies shows strong evidence that parsec-scale jets in FR0 sources are mildly relativistic with a bulk velocity on the order of 0.5c or less. A jet structure with a thin inner relativistic spine surrounded by a low-velocity sheath could be in agreement with the SMBH and jet launch region properties.

Key words. radio continuum: galaxies – galaxies: active – galaxies: jets

1. Introduction

It is now clear that most of the radio sources associated with low-redshift galaxies (e.g., Heckman & Best 2014) are compact, with corresponding linear sizes smaller than ~ 10 kpc (Baldi & Capetti 2009, 2010). These compact sources are located in red massive ($\sim 10^{11}$ solar masses) early-type galaxies, with high supermassive black hole (SMBH) masses ($\sim 10^8 M_{\odot}$), and spectroscopically classified as low-excitation radio galaxies (LERGs). They also show the same correlation between radio core power and [O III] line luminosity of FRIs, but are more core-dominated (by a factor of ~ 30) than FRIs and show a clear deficit of extended radio emission. For these reasons these compact sources were named FR0 (Ghisellini et al. 2011; Sadler et al. 2014; Baldi et al. 2015), being similar to FRI from the optical and nuclear radio emission point of view, but without an extended emission dominant at low frequencies.

The available information from observations of FR0s is still limited, even in the radio band, but recently major results have been obtained (see, e.g., JVLA observations presented in Baldi et al. 2015, 2019a). Most of the sources appear unresolved down to an angular resolution of ~ 0.3 arcsec, which corresponds

to 100–300 pc. A few sources show radio emission extended over a few arcseconds, on a scale of 2–14 kpc.

From an X-ray study of a sample of 19 FR0 radio galaxies Torresi et al. (2018) find that the X-ray photons are likely produced by the jet, as attested by the observed correlation between X-ray (2–10 keV) and radio (5 GHz) luminosities, similar to FRI radio galaxies. Overall, they find that the X-ray properties of FR0s are indistinguishable from those of FRIs. A comparison between FR0s and low-luminosity BL Lacs rules out important beaming effects in the X-ray emission of the compact radio galaxies.

A complete sample of FR0 radio galaxies have been selected from radio and optical surveys, the FR0CAT catalog (FR0CAT, Baldi et al. 2018) to constitute a workbench sample for the following studies of these compact radio-loud AGN. Thanks to LOFAR and GMRT observations of FR0 galaxies from the FR0CAT, Capetti et al. (2019, 2020) conclude that the fraction of FR0s showing evidence for the presence of jets at low radio frequencies, by including both spectral and morphological information, is at least $\sim 40\%$. This study confirms that FR0s and FRIs can be interpreted as two extremes of a continuous population of jetted sources (Capetti et al. 2017; Baldi et al. 2018), with the FR0s representing the low end in size and radio power.

Studying the properties and the origin of the radio emission in the most luminous, early-type galaxies (ETGs) in the nearby

[★] Reduced images are also available at the CDS via anonymous ftp to [cdsarc.cds.unistra.fr](ftp://cdsarc.cds.unistra.fr) (130.79.128.5) or via <https://cdsarc.cds.unistra.fr/viz-bin/cat/J/A+A/672/A104>

Universe with LOFAR observations, [Capetti et al. \(2022\)](#) found that about two-thirds of the detected ETGs are unresolved, with sizes on the order of 4 kpc or lower, confirming the prevalence of compact radio sources in local universe. Because these observations are at low radio frequencies, they exclude the presence of extended steep spectrum lobes and the authors conclude that these sources are FR0 candidates.

Various evolutionary scenarios were investigated (e.g., [Baldi et al. 2019a,b](#)). First, the possibility that all FR0s are young sources eventually evolving into extended sources was ruled out by the distribution of radio sizes. Similarly, a time-dependent scenario where accretion or jet launching properties prevent the formation of large-scale radio structures appears to be implausible, owing to the large abundance of subkiloparsec objects. Finally, a scenario in which FR0s are produced by mildly relativistic jets is consistent with the data, but requires observations of a larger sample to be properly tested.

[Garofalo et al. \(2010\)](#) discussed a model where powerful jets are due to fast spin retrograde accreting SMBHs, while a prograde configuration is identified with radio quiet galaxies. The natural time evolution of fast spin retrograde SMBHs is toward low-spin retrograde SMBHs followed by a prograde configuration ([Garofalo et al. 2016](#)). [Garofalo & Singh \(2019\)](#) identified a region of the jet power versus spin space corresponding to relatively weak jets (see their Fig. 1), possibly identified with FR 0 jets properties. Prograde low-spin BHs can shape compact and/or weak FR 0 jets.

[Massaro et al. \(2020\)](#) compared the properties of the large-scale environment, an orientation-independent property, of BL Lacs with those of samples of radio galaxies. This study revealed that BL Lacs are found in regions characterized by a significantly lower galaxy density with respect to FRIs, challenging predictions of the unification scenario (e.g., [Urry & Padovani 1995](#)). They noted that instead large-scale environments of BL Lacs are statistically consistent with those of the FR 0s. This implies that a substantial fraction of BL Lacs must be associated with FR0 sources oriented at a small angle from the line of sight and that FR0s are able to produce relativistic jets.

To test these suggestions VLBI observations of FR0s are necessary to check the presence of small scale jets and to study their properties and evolution. [Cheng & An \(2018\)](#) cross-matched the FR0CAT catalogue with the mJy imaging VLBA exploration at 20 cm (mJIVE-20) catalog and the Astrogeo database (see details and references in [Cheng & An 2018](#)). They found 14 FR0CAT sources with VLBI data, with fluxes at 1.4 GHz in the ~ 50 – 400 mJy range. In the VLBI images all of them show a radio structure. In four sources the high brightness temperature suggests Doppler boosting; in most of the sources the core emission is likely blended with that of the inner jet. They discuss that the VLBI properties of these FR0s are consistent with low-power compact symmetric object (CSO) properties, but observations of more FR0s are necessary to investigate this point. The authors noted that these 14 sources are more compact and brighter than the FR0 general population introducing possible selection effects.

In a follow up project, [Chen et al. \(2021\)](#) selected, from the 14 sources studied by [Cheng & An \(2018\)](#), the 8 FR0 that are resolved sources on parsec scale and without multi-epoch VLBI observations. They obtained EVN and VLBA data to investigate the presence of proper motions, to identify the core position, and to classify the radio source structure. In all eight sources they confirmed the presence of compact structures. In more detail: six sources show a two-sided morphology and two are one-sided jet sources. The low proper motion detected and the presence in

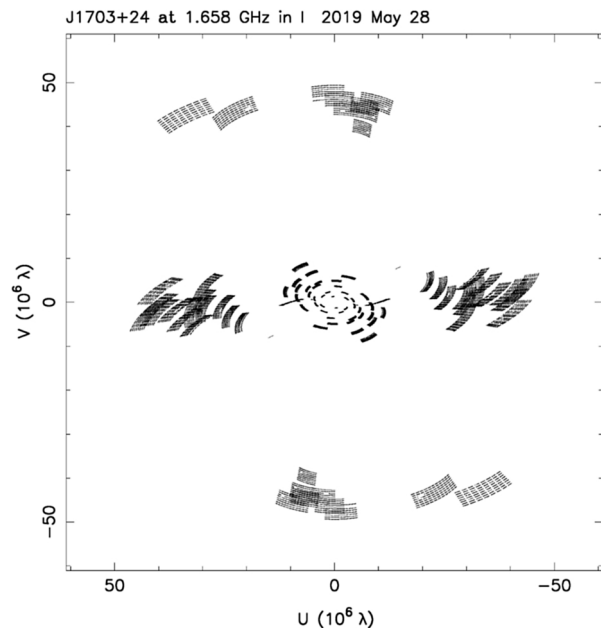


Fig. 1. uv -coverage for source J1703+24 observed with EVN.

most sources of a two-sided structure suggest a relatively large viewing angle and/or a low bulk velocity of FR0 jets.

[Baldi et al. \(2021\)](#) presented e-MERLIN observations of five FR0s and preliminary results from 1.7 GHz EVN observations of ten FR0s, which are discussed in more details here. The main result is that the large fraction of two-sided structures further support the presence of mildly relativistic jets in FR0s.

In this scenario we present here the results of EVN (at 1.7 GHz) and/or VLBA observations (at 1.5 and 5 GHz) of 18 FR0 sources. In Sect. 2 we describe these observations and discuss the data reduction. The results are presented in Sect. 3. In Sect. 4 we discuss FR0 parsec scale properties, and compare our results with the literature data. Our conclusions are presented in Sect. 5.

The intrinsic parameters quoted in this paper are computed assuming a Λ CDM cosmology with $H_0 = 70 \text{ km s}^{-1} \text{ Mpc}^{-1}$, $\Omega_m = 0.3$, and $\Omega_\Lambda = 0.7$.

2. Observations and data reduction

Among the 25 FR0s studied with JVLA observations in the A array ([Baldi et al. 2015, 2019a](#)), we selected sources with a core flux density at 1.4 GHz greater than 20 mJy and $z < 0.05$. The 11 sources selected were observed with EVN at 1.7 GHz. Observations were carried in May 2019 in phase reference mode with a data rate of 1024 Mbit/sec (project EG100). Nearby phase calibrators selected from the VLBA calibrator list, and target sources were observed with a ~ 5 min cycle. The total observing time was ~ 2 h/source with at least 60 min on the target source and the remaining time on calibrator source and motion. Data were correlated at the JIVE correlator in Dwingeloo. In Fig. 1 we show the typical uv -coverage obtained using the following array: Jodrell (Lovell), Westerbork single antenna, Effelsberg, Medicina, Onsala 25m, Urumqi, Torun, Hartebeesthoek, Svetloe, Zelenchukaskaya, Badary, and Irbene. Data calibration was carried out in the standard mode using the EVN pipeline. Data reduction was done in AIPS, using the task IMAGR to obtain images. Self-calibration in phase was applied (when possible because of the low correlated flux density) to improve the

Table 1. Observational parameters.

Name	EVN 1.7 HPBW mas	EVN 1.7 noise $\mu\text{Jy beam}^{-1}$	VLBA 1.5 HPBW mas	VLBA 1.5 noise $\mu\text{Jy beam}^{-1}$	VLBA 5 HPBW mas	VLBA 5 noise $\mu\text{Jy beam}^{-1}$
J0020-00	–	–	8 × 4	59	2.5 × 2.5	17
J0115+00	–	–	10 × 4	46	3 × 2	18
J0907+32	15 × 7	50	10 × 10 15 × 15	77 54	4 × 3	17
J0930+34	16 × 9(–8)	35	–	–	–	–
J0943+36	17 × 7(–25)	198	–	–	–	–
J1025+10	21 × 11(–5)	100	–	–	–	–
J1040+09	20 × 20	120	14 × 13	15	5 × 5	20
J1136+51	–	–	13 × 8(–20)	50	4 × 2.5	30
J1213+50	25 × 25	270	–	–	–	–
J1230+47	24 × 15	140	–	–	–	–
J1530+27	21 × 12(–10)	400	–	–	–	–
J1559+25	15 × 10(–25)	70	–	–	–	–
J1621+25	–	–	12 × 12	50	2.5 × 2.5	30
J1628+25	20 × 12(–40)	100	4 × 3.5	35	0.9 × 0.9	17
J1658+25	–	–	6 × 6	37	2.5 × 2.5	31
J1703+24	15 × 10(–14)	50	5 × 3	29	3 × 2	25
J2336+00	–	–	10 × 10	30	5 × 3	40
J2346+00	–	–	5 × 5	28	2 × 2	15

Notes. Col. 1: source name; Col. 2: EVN HPBW at 1.7 GHz, the orientation angle is in parentheses, if not reported it is at zero degree or it is a circular beam; Col. 3: noise level (1σ) of EVN images at 1.7 GHz; Col. 4: VLBA HPBW at 1.5 GHz, the orientation angle is in parentheses, if not reported it is at zero degree or it is a circular beam; Col. 5: noise level (1σ) of VLBA images at 1.5 GHz; Col. 6: VLBA HPBW at 5 GHz, the orientation angle is in parentheses, if not reported it is at zero degree or it is a circular beam; Col. 7: noise level (1σ) of VLBA images at 5 GHz.

quality of the images. The final parameters are reported in the next section.

Moreover, in the time range September–December 2021 we observed 11 FR0s with the VLBA at 5 and 1.5 GHz (project BG272). Selected sources are characterized by a complex and steep radio spectrum in the high-frequency range, with a flatter or self-absorbed spectrum in the low-frequency range. Sources were observed in phase-reference mode at 5 and 1.5 GHz for 2 h each including calibration and dwell time. After the correlation at the NRAO Socorro correlator, data were imported in AIPS and calibrated using the standard technique. Images were produced using the AIPS task IMAGR; bad data were flagged mostly thanks to the task TVFLG; self-calibration in phase only was applied when possible to improve the image quality. Dual frequency observations are useful to properly identify the radio core and turbulence regions using spectral index information and comparing different source morphology; we have high-resolution images of the source core and lower resolution, high-sensitivity images of the diffuse steep spectrum regions. In Fig. 2 the typical uv -coverage of a source at the two frequencies is shown.

3. Results

In Table 1 we present the parameters of the images obtained from these observations and in Table 2 we present estimated source parameters from the images. The core structure was identified from spectral index information, when available. In other sources it was identified with the brightest compact component. More details are reported in the next subsection (comments on the individual sources). Core parameters were measured using the task JMFITS in AIPS. This task fits up to four Gaussian components to a portion of an image. The starting model is a

Gaussian with a width equal to the half power beam width of the image, centered on the peak of the component. In most sources a convergence is obtained after 40–50 iterations. In diffuse sources we integrated the flux density within the 2σ area to avoid negative regions. We checked that the total flux density is not sensitive to a larger integration area. The source size is obtained from the deconvolved Gaussian fit in slightly extended regions, while it is directly measured on the image for well-resolved sources. The size uncertainty is 0.1 times the HPBW for unresolved or slightly extended sources (Gaussian fit) and ~ 0.3 times the HPBW in resolved sources. The source PA uncertainty is a few degrees. We note that we produced images with a redundant cell size, approximately ten times smaller than the HPBW, for a better quality of the images. The flux density uncertainty was obtained combining the image noise level reported in Table 1 with the gain calibration uncertainty as

$$\Delta S = ((0.03 \times S)^2 + \text{noise}^2)^{0.5},$$

where S is the flux density; the calibration uncertainty has been evaluated at $\sim 3\%$. We note that, given the low flux density of most of our sources, the density flux uncertainty is noise dominated. In a few sources the flux density uncertainty can be higher because of a peculiar source structure or other problems commented on in single source notes (Sect. 3.1).

Images of resolved sources are in Figs. 3–15. No image is presented for unresolved sources since they appear as a beam image and no information (e.g., field sources or noise structures) is present. Single sources are discussed in Sect. 3.1 where more details are presented.

Table 3 provides the source parameters of our sample. The jet-to-counter-jet ratio, reported in Col. 5 is the ratio of the surface brightness of the two opposite jets in the region near the VLBI core, $R_{\text{JC}} = F_{\text{jet}}/F_{\text{cjet}}$. When the counter-jet was not

Table 2. Source data.

Name	RA Dec	z	EVN 1.7 core(mJy) total(mJy)	VLBA 1.5 core(mJy) total(mJy)	VLBA 5 core(mJy) total(mJy)	LAS mas pc	PA deg	Note
J0020-00	00 20 34.700 -00 28 14.40	0.0720	–	0.94(0.07) 1.48(0.08)	0.35(0.02) 0.82(0.03)	10 14	160 140	One-sided
J0115+00	01 15 15.702 00 12 48.59	0.0450	–	7.26(0.05) 38.42(1.10)	5.77(0.02) 35.34(1.00)	40 35	95	Two-sided
J0907+32	09 07 34.827 32 57 22.80	0.0490	–	0.45(0.05) 13.28(0.70)	<0.04 ND	65 62	80	Double+core Spiral galaxy
J0930+34	09 30 03.560 34 13 25.34	0.0420	–	–	–	15 12	90	Double Structure
J0943+36	09 43 19.159 36 14 52.07	0.0223	140(7.0)	–	–	P	–	Unresolved Variable
J1025+10	10 25 44.213 10 22 30.48	0.0457	106(5.0)	–	–	P	110	See text
J1040+09	10 40 28.373 09 10 57.25	0.0195	–	2.45(0.20) 14.57(0.74)	3.08(0.25) 5.68(0.28)	90 36	180	Two-sided Complex
J1136+51	11 36 37.148 51 00 08.44	0.0498	–	1.43(0.05)	0.30(0.03)	P	–	Unresolved Steep spectrum
J1213+50	12 13 29.280 50 44 29.38	0.0308	–	–	–	15 9	145	See text
J1230+47	12 30 11.852 47 00 22.63	0.0391	11.85(0.83) 68.8(2.1)	–	–	100 77	0	Two-sided Symmetric
J1530+27	15 30 16.153 27 05 51.01	0.0325	48.5(2.4) 62.6(3.1)	–	–	15 10	65	One-sided?
J1559+25	15 59 51.615 25 56 26.33	0.0447	6.98(0.71)	–	–	P	–	See text
J1621+25	16 21 46.069 25 49 14.45	0.0480	–	0.50(0.06) 5.95(0.19)	0.28(0.03) 0.30(0.03)	180 169	90 130	Two-sided z -shaped
J1628+25	16 28 46.129 25 29 40.97	0.0401	–	8.27(0.31) 27.4(1.4)	7.94(0.28) 26.50(0.80)	12 10	115-90	2-sided
J1658+25	16 58 30.054 25 23 24.97	0.0327	–	6.51(0.10) 13.83(0.17)	10.26(0.16) 12.94(0.16)	73 48	60	2-sided distorted
J1703+24	17 03 58.503 24 10 39.52	0.0310	4.00(0.20) 11.00(0.55)	?? 9.34(0.30)	?? 3.46(0.15)	40 25	70?	Core? Complex
J2336+00		0.0763	–	ND	ND	–	–	Not detected
J2346+00	23 46 09.103 00 59 08.83	0.0927	–	4.61(0.25) 23.91(0.72)	2.00(0.21) 9.84(0.30)	30 52	105	2-sided z -shaped

Notes. Col. 1: source name; Col. 2: core position obtained with a gaussian fit; Col. 3: source redshift; Cols. 4,5,6: core (top) and total (bottom) flux density in mJy in the different available images; Col. 7: largest measured size of the source in mas (top) and parsec (bottom); Col. 8: source orientation in the image in degrees; Col. 9: comments.

detected we report an upper limit obtained using the one-sigma noise level as counter-jet surface brightness. In other sources the ratio uncertainty is in parentheses; it does not affect observed beaming effects.

3.1. Comments on the individual sources

J0020-00. This source shows a two-sided symmetric structure in the JVLA image at 7.5 GHz published in Baldi et al. (2015). eMERLIN show a core with scattered components along the JVLA radio axis Baldi et al. (2021). In the VLBA images it shows (Fig. 3) a one-sided structure at 1.5 GHz at PA = 140° (the same as the arcsec structure) and an inner core in the VLBA image at 5 GHz with a symmetric short extension along PA 160°. The jet-to-counter-jet ratio at 1.5 GHz is >2.7. The JVLA core flux density at 7.5 GHz is significantly lower than the correlated flux density at 1.5 GHz (the ratio is

1.59), suggesting variability and/or complex nuclear spectral index.

J0115+00. This source, unresolved in JVLA images (Baldi et al. 2015), shows a symmetric two-sided structure in VLBA images at 1.5 (Fig. 4) and 5 GHz. The ratio of the VLBA correlated flux at 1.5 GHz to the JVLA flux density at 7.5 GHz is 1.05, suggesting that in the VLBA image all the nuclear structure is visible. The jet-to-counter-jet ratio is ~1. The source spectrum in both the JVLA and VLBA images is flat.

J0907+32. This peculiar source is identified with a spiral galaxy and should not be included among the FR0 sources. However, because of its peculiar structure we report here data and images. We do not use it in statistical considerations. A similar source (B2 0722+30) was found by Liuzzo et al. (2013), who studied a sample of compact FRI sources. In JVLA images (Baldi et al. 2019a) J0907+32 shows a nuclear emission and a

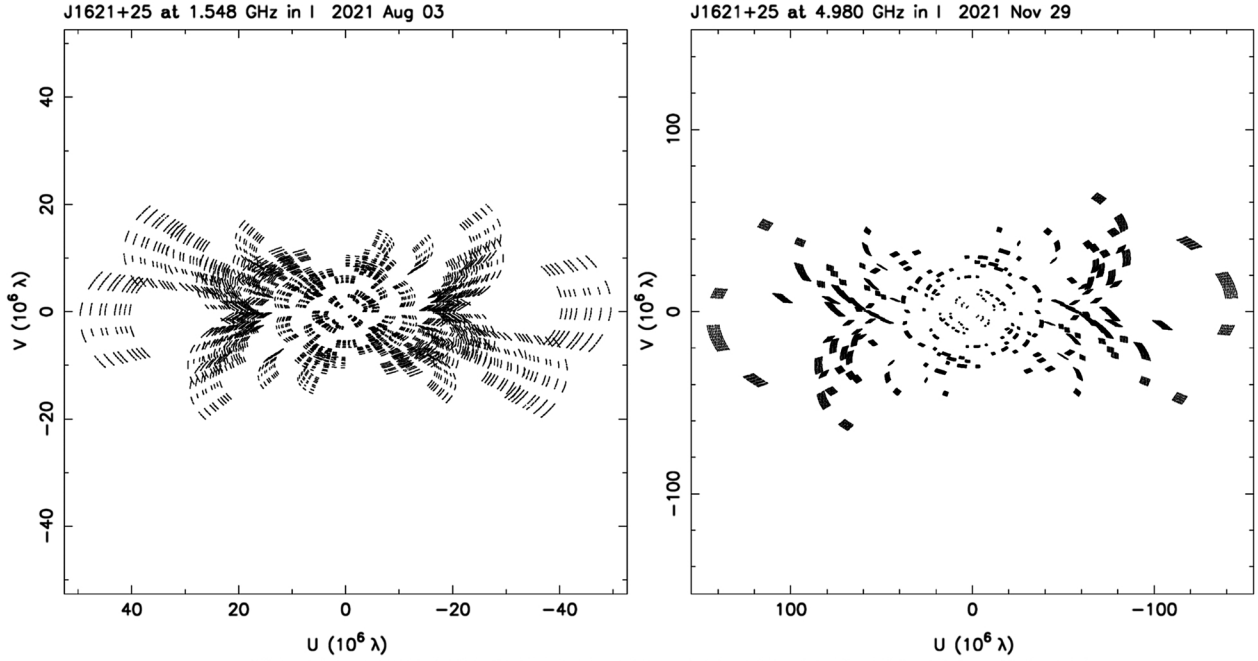


Fig. 2. *uv*-coverage for source J1621+25 observed with VLBA at 1.5 GHz (left) and at 5 GHz (right).

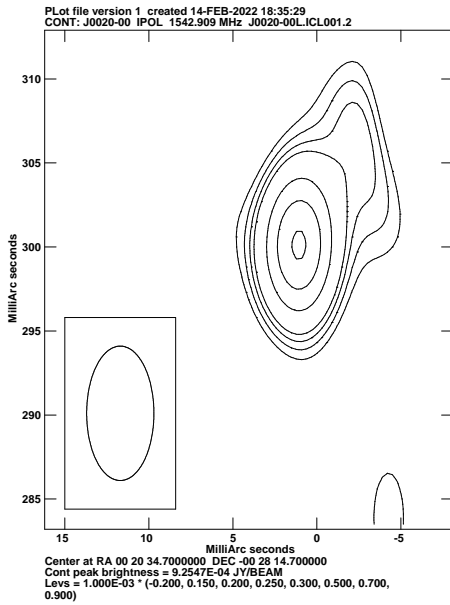


Fig. 3. Contour image of J0020-00 obtained with VLBA at 1.5 GHz.

symmetric structure identified with the disc emission easily confused with two-sided jets. Interestingly the nuclear emission is slightly resolved in the direction perpendicular to the disk. EVN images at 1.7 GHz and VLBA at 1.5 GHz shows two symmetric small-scale lobes in agreement with the nuclear arcsecond extension perpendicular to the disk. In the VLBA image a possible central emission is present (Fig. 5). The VLBA data at 5 GHz completely resolve this structure and no significant structure is visible. It is a puzzling steep spectrum source, suggesting AGN activity in the core of this spiral galaxy but with no jet-like structure. The presence of a similar structure in B2 0722+30, as noted before, could suggest the possibility of FR0-like structures in a

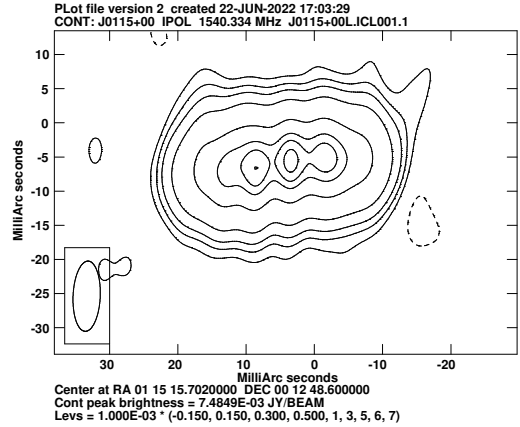


Fig. 4. Contour image of J0115+00 obtained with VLBA at 1.5 GHz.

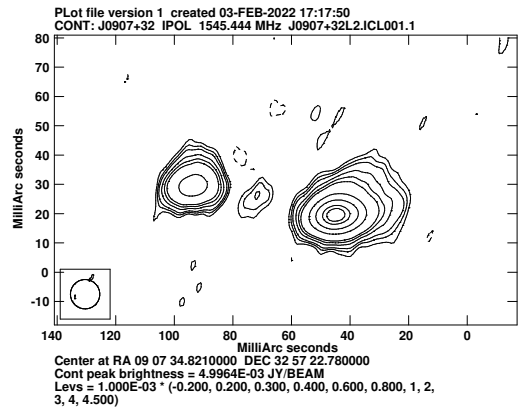


Fig. 5. Contour image obtained with VLBA at 1.5 GHz of J0907+32.

few cores of spiral galaxies. More data are necessary to discuss this point.

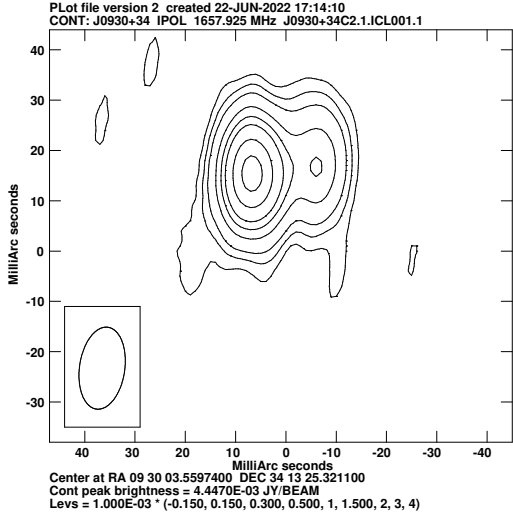


Fig. 6. Contour image of J0930+34 obtained with EVN at 1.7 GHz.

J0930+34. This source, unresolved but with a steep spectrum in JVLA observations (Baldi et al. 2019a), is resolved in EVN observations in a double structure (Fig. 6). The core identification is not clear; we note that the correlated flux density is significantly lower than the JVLA flux density at 7.5 GHz. The ratio is 0.57, due to the source steep spectrum and a possibly missing structure in VLBI image. In any case, if the stronger lobe (5.42 mJy) is the core and the secondary lobe (1.76 mJy) a one-sided jet, the jet-to-counter-jet ratio does not require a fast jet ($v > 0.4c$).

J0943+36. This source is unresolved in our EVN observations and in VLBA observations at 8 GHz (Cheng & An 2018). The source flux density is 140 mJy and in the image no dynamic range problem is present. The unresolved source is the only visible structure, also in large field images. The radio spectrum is inverted and it shows evidence of variability. This property and the relatively high radio power suggest a relativistic source oriented at a small angle from the line of sight. The ratio of the correlated EVN flux density to the JVLA flux density at 7.5 MHz (Baldi et al. 2019a) is 0.50. This can be due to an inverted spectrum and source variability.

J1025+10. Unresolved in EVN observations at 1.7 GHz, it is resolved with a two-sided structure (13 pc in size) in the EVN 5 GHz image by Cheng et al. (2021). In their image the inner core is extended at PA = 90° and the two-sided jets are at PA 130°, suggesting a Z-shaped structure in the inner (~1 pc) region. The source size in the 5 GHz image is in agreement with the unresolved structure at 1.7 GHz. In our image no dynamic range problem is present. The unresolved source is the only visible structure, also in large field images. The core flux density ratio of the EVN correlated flux to the JVLA flux density at 7.5 GHz (Baldi et al. 2019a) is 0.92. The radio spectrum from the total flux density estimated with JVLA is peaked at 5 GHz in agreement with the source's small size.

J1040+09. This is a very complex source. The VLBA image at 5 GHz shows an unresolved core, a northern curved jet, and some structure in the south (Fig. 7, top panel). At 1.5 GHz the core is surrounded by a diffuse emission; the northern jet is extended ~20 mas, transversely resolved, while the southern jet is extended ~60 mas and it is heavily transversely resolved (Fig. 7, bottom panel). The classification of the structure as a

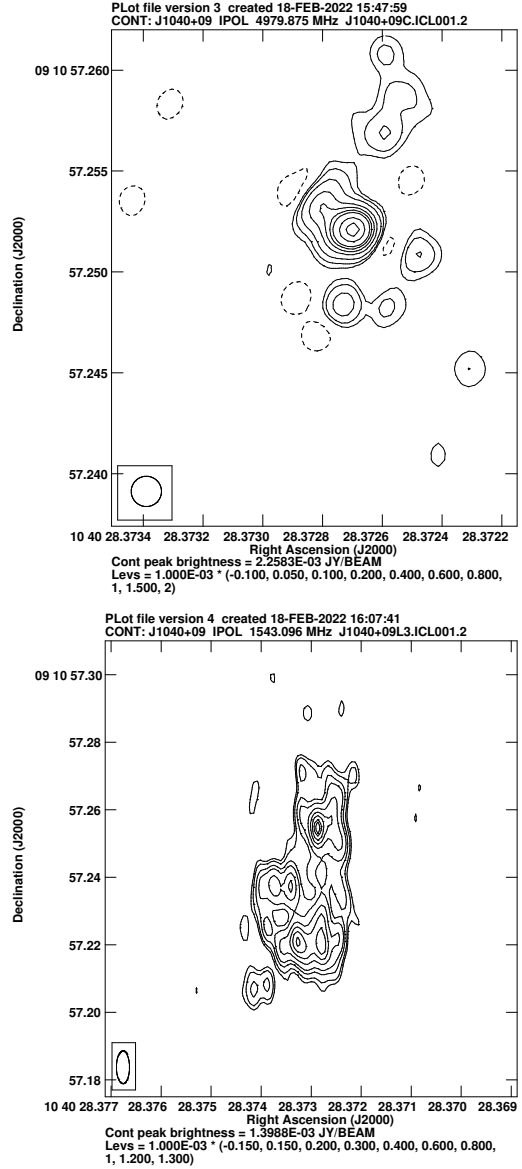


Fig. 7. Contour image of J1040+09 obtained with VLBA at 5 GHz (top) and at 1.5 GHz (bottom).

jet is uncertain; it could be a parsec-scale lobe, given its size of 15.80×8.7 pc (PA 180°). Lower resolution images confirm this structure, with a slightly larger size. The comparison between the correlated VLBI flux density and the flux density of the unresolved source imaged by JVLA at 7.5 GHz (Baldi et al. 2019a) is 0.77.

Because of the low correlated flux, no self-calibration was possible. We carefully edited the data and compared the 1.5 and 5 GHz images with the same uv -range and angular resolution between the images shown here. In these images the radio structures are in agreement; therefore, we are confident that the observed complex structure is real.

J1136+51. This is an unresolved source with a steep spectrum, $\alpha_{1.5}^5 = 1.3$, which could be an old source. No other radio source is visible, even in large field images. The ratio of the VLBI correlated flux to the JVLA flux density (Baldi et al. 2019a) is 1.22.

J1213+50. This is a slightly extended source with a nearly symmetric structure in the EVN image at 1.7 GHz (Fig. 8). The

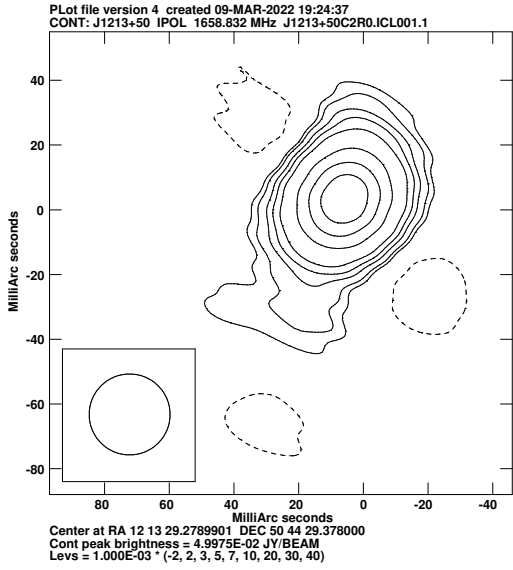


Fig. 8. Contour image of J1213+50 obtained with EVN at 1.7 GHz.

source extension is at PA 145° , but at PA 0° in the JVLA 5 GHz image (Baldi et al. 2019a) and 90° in the VLBA 8 GHz image by Cheng & An (2018). No jet boosting is evident in all images. The core flux density ratio is 0.74.

J1230+47. The extended symmetric structure in the EVN images at 1.7 GHz is more than 70 pc in size (Fig. 9). The central core is resolved in the images by Cheng & An (2018) in a two-sided structure 7–8 pc in size at the same PA of the more extended structure, suggesting a possible recurrent activity. The source is unresolved in JVLA images by Baldi et al. (2019a).

J1530+27. A core dominates in the EVN images at 1.7 GHz with a short one-sided emission (Fig. 10) possibly identified with a jet. Because of the low brightness of this structure, Doppler boosting is not evident. The JVLA flux densities show an unresolved self-absorbed structure with the highest flux density at 5 GHz (Baldi et al. 2019a).

J1559+25. This source is one-sided in JVLA images (Baldi et al. 2019a) with a jet size of 3 kpc; it is unresolved in our EVN data, but one-sided in the 8 GHz VLBA image by Cheng & An (2018). The parsec- and kiloparsec-scale structure are at the same PA. The jet is transversely resolved in the VLBA image. The jet-to-counter-jet ratio in the VLBA image is higher than 6. The minimum velocity is $0.34c$ and the maximum orientation angle is 70° .

Our image is not affected by dynamic range problems. No other radio structure is visible, even in large field images.

J1621+25. In the 5 GHz and 1.5 GHz high-resolution VLBA images this source shows a short (28 pc in size) symmetric nuclear structure at PA $= 90^\circ$. At lower resolution (HPBW = 12×12 mas), a symmetric complex double-jet structure ~ 170 pc in size is clearly evident at PA 130° . The jet is transversely resolved and its extension is noise limited (see Fig. 11). The correlated flux density is 2.7 times the unresolved core estimated at 7.5 GHz in JVLA data by Baldi et al. (2019a), suggesting an extended steep spectrum structure.

J1628+25. This source is unresolved in JVLA high-resolution images (Baldi et al. 2019a) and in the EVN image. At higher resolution (VLBA images) it is resolved in a symmetric structure. The inner 10 pc are in PA 115° (1.5 and 5 GHz image),

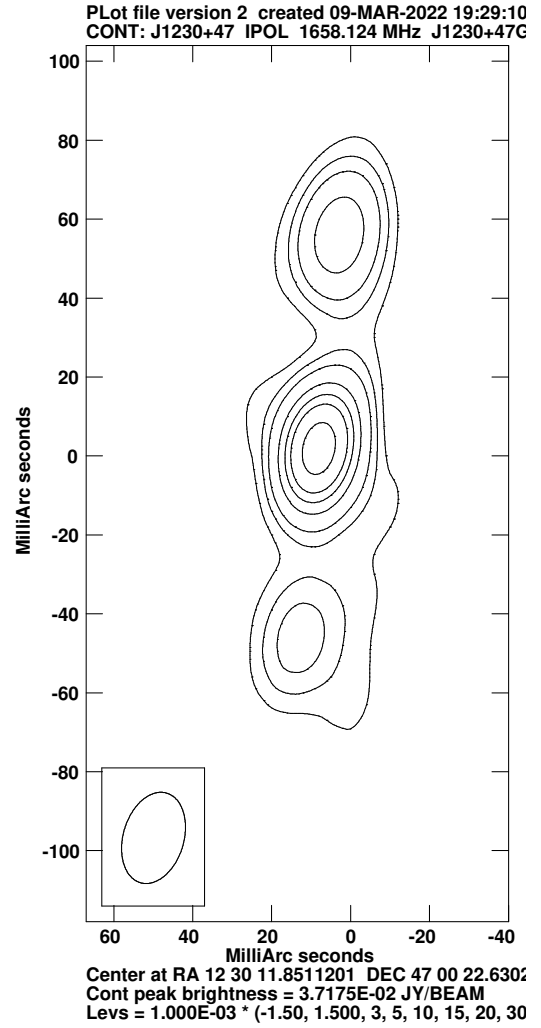


Fig. 9. Contour image of J1230+47 obtained with EVN at 1.7 GHz.

but the more external regions visible only at 1.5 GHz rotate to a PA $\sim 90^\circ$ (Fig. 12).

J1658+25. Two-sided jets are present in the VLBA 1.5 GHz image (Fig. 13) slightly bent with respect to the inner structure. In the 5 GHz VLBA image (not shown here) only a slightly extended core emission is visible. The correlated VLBA flux is in agreement with the JVLA flux density by Baldi et al. (2019a).

J1703+24. This is a complex source. In the VLBA images we see a complex two-sided structure oriented in E-W (Fig. 14, top panel). In the EVN image a symmetric two-sided structure is confirmed, but at a different PA: 70° (Fig. 14, bottom panel). We note that the JVLA PA is $\sim 110^\circ$ (Baldi et al. 2019a). The source is detected also in LOFAR observations (Capetti et al. 2020) and it is slightly extended (5–6 kpc), in agreement with the JVLA image.

To confirm this complex structure we self-calibrated in phase only our data at 1.5 and 1.7 GHz. Self-calibrated images have a better noise level; the source structure is confirmed. We also compared images at different frequencies at different angular resolution using the same uv -range (cutting long or short baselines). The present results are in agreement with all the tests we performed.

J2336+00. We did not detect this source with VLBA at 1.5 and 5 GHz. This could be due to a bad choice of the phase

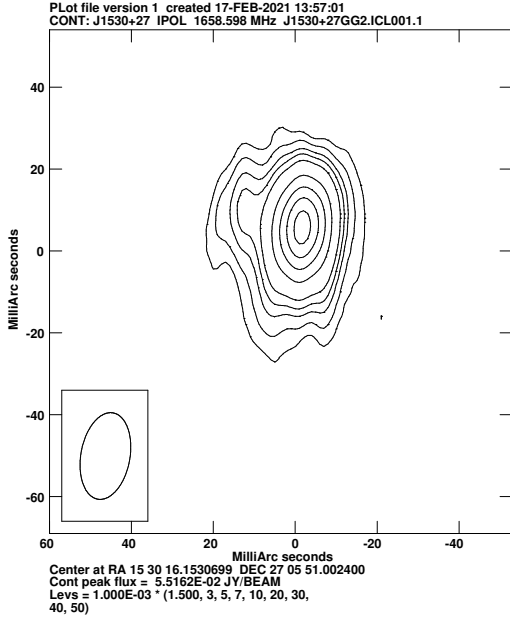


Fig. 10. Contour image of J1530+27 obtained with EVN at 1.7 GHz.

calibrator (J2340-0053), too faint and resolved. However, this source has been slightly resolved by eMERLIN (Baldi et al. 2021), which shows a core of $0.64 \text{ mJy beam}^{-1}$ with a weaker second component. Moreover, the target source is resolved in JVLA observations (Baldi et al. 2015) with a faint nuclear emission (1.96 mJy , at 7.5 GHz) with a steep spectrum: 1.00 between 1.4 and 7.5 GHz suggesting a faint resolved core.

J2346+00. We observed this source with the VLBA at 1.5 and 5 GHz . The images show a two-sided symmetric emission $\sim 50 \text{ pc}$ in size. The inner nuclear emission ($\sim 10 \text{ pc}$) is at PA $\sim 90^\circ$; the two-sided extended jet emission is at PA 105° , suggesting a Z-shaped structure (Fig. 15). It is unresolved in JVLA images by Baldi et al. (2015).

3.2. Other sources

VLBI observations of FR0 sources not included here have been mostly presented in Cheng & An (2018) and Cheng et al. (2021). We already quoted their results for the sources in common with our sample; here we briefly report their results for sources not present in our sample to increase our knowledge of FR0 parsec-scale jets.

J0906+41. This is a core-dominated source with a two-sided symmetric structure. The ratio of the NVSS flux density at 1.4 GHz to the total correlated flux density at 8.4 GHz is ~ 1.7 – 1.8 suggesting an inverted radio spectrum. The jet-to-counter-jet ratio is low, 3.9 , and no relativistic boosting is necessary.

J0909+19. This is a two-sided source; the southern jet shows a large bend, from PA 180° to PA 110° (see Cheng & An 2018; Cheng et al. 2021). The 8.4 GHz correlated flux (104.5 mJy in Cheng & An 2018 and 156 mJy in Cheng et al. 2021) is significantly higher than the NVSS flux density (69.1 mJy), suggesting an inverted radio spectrum and/or a source variability.

J0910+18. This is a point-like source in the VLBA 8 GHz image (Cheng & An 2018); it shows a diffuse low-brightness halo structure in a LOFAR image (Capetti et al. 2020). No connection is evident between the central structure and the halo low-

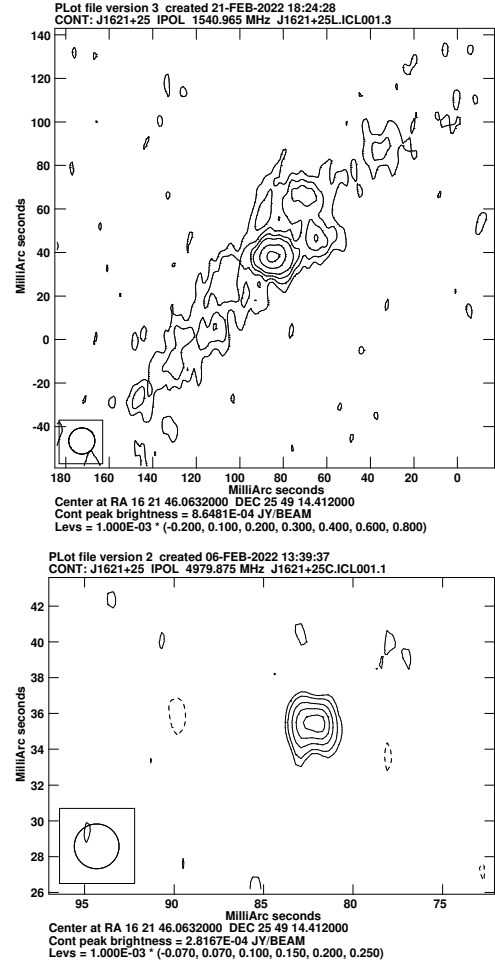


Fig. 11. Contour image of J1621+25 obtained with VLBA at 1.5 GHz (top) and 5 GHz (bottom).

brightness structure, suggesting that the diffuse low-brightness emission is the remnant of a previous activity. This structure shows a relatively steep radio spectrum ($\alpha = 0.96$): 480.7 mJy at 150 MHz (Capetti et al. 2020) and 50 mJy at 1.4 GHz (NVSS).

J0933+10. This is a one-sided source. The ratio of the correlated VLBI flux to NVSS is only ~ 0.6 , suggesting a missing structure in VLBI images. The jet-to-counter-jet ratio is >8 .

J1037+43. This is a one-sided core dominated structure (Cheng et al. 2021). The correlated flux is significantly lower than the NVSS source flux density (the ratio is ~ 0.2), suggesting the presence of a missing structure in VLBI images and/or source variability. The jet-to-counter-jet ratio is >20.8 ; assuming that it is due to Doppler relativistic beaming, it requires a velocity larger than $0.54c$ and an angle smaller than 57° .

J1205+20. In images by Cheng & An (2018) and Cheng et al. (2021), this source shows a one-sided jet and a diffuse lobe-like structure on the other side. The correlated flux is 41.2 mJy at 8.4 MHz and the NVSS flux density is 89.9 mJy . The jet-to-counter-jet ratio near the core is ~ 33 ($v > 0.6c$ and $\theta < 50^\circ$). The spectral index of the diffuse NE structure is 0.75 or steeper. It could be the remnant of a previous activity and/or a peculiar structure related to the counter-jet interaction with the ISM.

J1246+11. This is a one-sided jet structure in Cheng & An (2018). The source flux density in the NVSS is 61.2 mJy , 38 mJy in Cheng & An (2018) at 8 GHz and only 7 – 8 mJy in

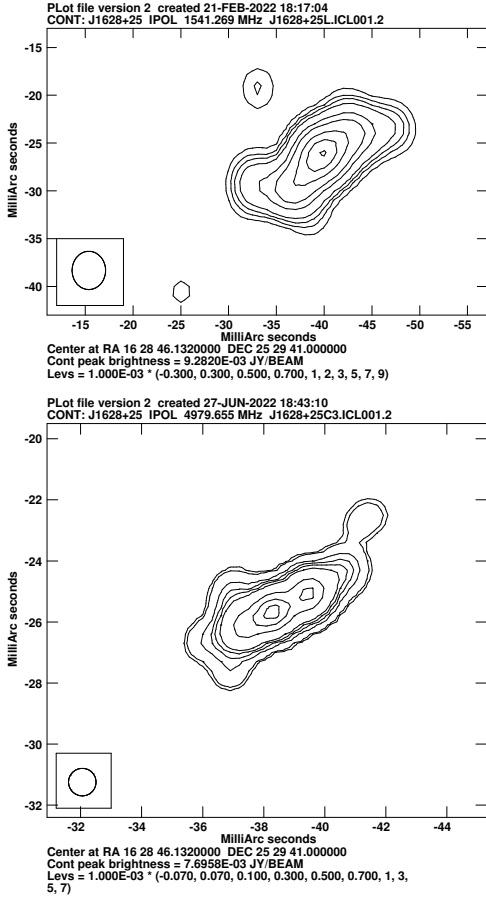


Fig. 12. Contour image of J1628+25 obtained with VLBA at 1.5 GHz (top) and 1.5 GHz (bottom).

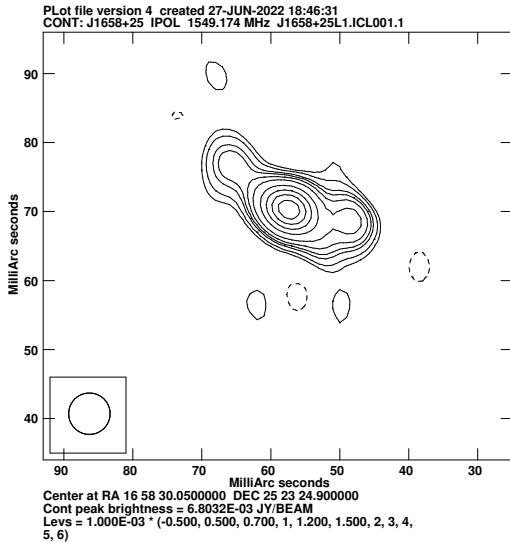


Fig. 13. Contour image of J1658+25 obtained with VLBA at 1.5 GHz.

Cheng et al. (2021) at 5 and 8 GHz. More observations are necessary to understand this source.

J1604+17. Only a core-like structure is visible in the image reported by Cheng & An (2018), even if in the table it is reported as a jet-like structure. The correlated flux is in agreement with the NVSS flux density measure for this source. A tail-like struc-

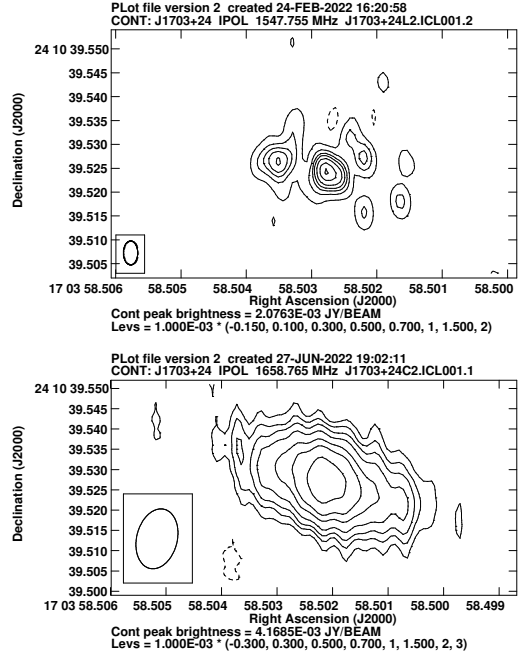


Fig. 14. Contour image of J1703+24 at 1.5 GHz with VLBA (top) and EVN at 1.7 GHz (bottom).

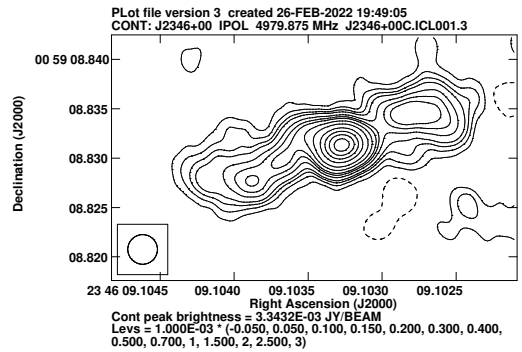


Fig. 15. Contour image of J2346+00 at 5 GHz (VLBA).

ture interacting with a nearby galaxy is present in the LOFAR image in Capetti et al. (2020).

J1606+18. A one-sided source is reported in Cheng & An (2018). The correlated flux density is 360 mJy; the NVSS flux density is 396 mJy. The jet-to-counter-jet ratio is >8 .

NGC5322. This source at $z = 0.00594$ was studied by Feretti et al. (1984) and more recently by Dullo et al. (2018). The source shows a two-sided symmetric extended jet structure.

NGC1052. This source at $z = 0.00496$ is a well-known active radio galaxy because of its low redshift. Baczkowski et al. (2022) confirms the presence of a remarkably straight low-velocity double-sided jet.

4. Discussion

The low radio power and the lack of a kiloparsec-scale radio emission in FR0 sources could suggest an origin of the radio emission different from the classic non-thermal emission from a SMBH and jets, for example star formation or a disc-corona wind emission, similarly to what has been suggested for radio quiet AGN (e.g., Panessa et al. 2019). The widespread detection

Table 3. Source properties.

Name	Log P_{tot} (ν) W Hz $^{-1}$	Log P_{core} (ν) W Hz $^{-1}$	$S_{\text{VLBI}}/S_{\text{core-JVLA}}$	Jet-to-cjet ratio
J0020-00	22.75 (1.5)	21.65 (5.0)	1.59	>2.7
J0115+00	23.26 (1.5)	22.44 (5.0)	1.05	1 (0.1)
J0907+32	22.88 (1.7)	21.41 (1.5)	3.34	1 (0.2)
J0930+34	22.47 (1.7)	–	0.57	>10
J0943+36	–	23.20 (1.7)?	0.50	–
J1025+10	23.72 (1.7)	–	0.92	–
J1040+09	22.22 (1.5)	21.42 (5.0)	0.77	1 (0.2)
J1136+51	21.92 (1.5)	21.25 (5.0)	1.23	–
J1213+50	23.08 (1.7)	–	0.74	1 (0.1)
J1230+47	23.39 (1.7)	22.63 (1.7)	1.35	1.4 (0.1)
J1530+27	23.18 (1.7)	23.07 (1.7)	1.39	>8
J1559+25	–	22.57 (1.7)	0.52	–
J1621-25	22.51 (1.5)	21.18 (5.0)	2.70	1 (0.1)
J1628+25	23.02 (1.5)	22.47 (5.0)	1.14	1 (0.1)
J1658+25	22.53 (1.5)	22.40 (5.0)	1.01	1 (0.1)
J1703+24	22.39 (1.7)	???	0.44	1 (0.1)
J2236+00	–	–	...	–
J2346+00	23.71 (1.5)	22.64 (5.0)	2.63	1 (0.1)

Notes. Col. 1: source name; Col. 2: total radio power in W Hz $^{-1}$, in parentheses the observed radio frequency in GHz; Col. 3: core radio power in W Hz $^{-1}$, in parentheses the observed radio frequency in GHz; Col. 4: the ratio of the correlated VLBI flux density to the core flux density in JVLA observations; Col. 5: the jet-to-counter-jet surface brightness ratio in the region near to the VLBI core, the ratio uncertainty is in parentheses.

of compact parsec-scale jets in FR0s indicates that the origin of the radio emission is synchrotron emission from outflows produced by a SMBH at the center of the parent galaxy.

4.1. The jet-to-counter-jet ratio

The jet-to-counter-jet ratio, $R_{\text{JC}} = F_{\text{jet}}/F_{\text{cjet}}$, can be ascribed to the relativistic boosting of two otherwise symmetric jets (see, e.g., Giovannini 2004). Therefore, this parameter can be linked to the jet bulk speed, and it is very useful to study the jet velocity distribution. To this end, Giovannini et al. (2005) selected a sample of radio galaxies from the B2 Catalogue of Radio Sources and the Third Cambridge Revised Catalog (3CR), forming the Bologna Complete Sample (BCS), with no selection constraint on the nuclear properties. The jet-to-counter-jet ratio distribution of the BCS sources was discussed by Liuzzo et al. (2009a), who found that $\sim 30\%$ of the sources show evidence of a two-sided structure. This result is in agreement with a jet velocity of $\beta \sim 0.9$, and a random orientation of radio galaxies with respect to our line of sight.

In new sources presented here and in the literature data (see Sects. 3.1 and 3.2), we find that 56% of FR0s show a two-sided structure (52% if we exclude NGC5322 and NGC1052). The FR0 sample with VLBI observations is not a complete sample, but it is representative of the parsec-scale structures of this class of sources if we take into consideration selection effects. Only sources with an unresolved nuclear emission in JVLA images larger than 20 mJy at 1.4 GHz (see Sect. 2) were selected for EVN observations. Moreover, sources observed by Cheng & An (2018) have a higher nuclear flux density with respect to the general FR0 population. These selection biases in our sample favor sources whose nuclear emission is boosted by Doppler beaming, that is, those seen at a smaller angle with respect to the line of sight. Therefore, we would expect as selection effect a lower percentage of two-sided structures with respect to a sample of randomly distributed sources as the BCS. Conversely, the

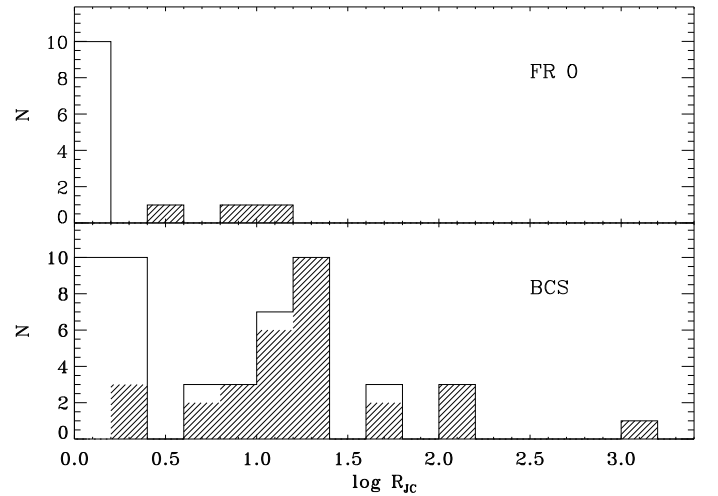


Fig. 16. Distributions of the logarithm of the ratio R_{JC} between the flux densities of the jet and counter-jet for the FR0s (top panel) and the source in the BCS sample (bottom panel). The dashed portions of the histograms correspond to lower limits on R_{JC} .

percentage of two-sided sources (56%) found here is significantly higher than the 30% found in the sample by Liuzzo et al. (2009a).

We conclude that the high percentage of FR0 with a two-sided structure is strong evidence that parsec-scale jets in FR0 sources are mildly relativistic or not relativistic ($v \sim 0.5c$ or lower). The lower bulk speed of the jets in FR0s with respect to the BCS sources is also supported by the distribution of the jet-to-counter-jet ratio for the two samples presented in Fig. 16. The fraction of FR0s with $R_{\text{JC}} > 2$ is 23%, while this fraction is between 60% and 66% (depending on the actual values of the lower limits) in the FRIs. By considering the upper limits, the mean values of the two distributions (Kaplan Meier estimator)

are 2.7 ± 1.0 and 1.2 ± 0.2 for BCG galaxies and FR0s, respectively. The probability that the two populations are drawn from different distributions of R_{1C} is $>98\%$ ¹. Furthermore, because the FR0s sample is biased toward sources seen at a smaller angle with respect to the line of sight, this difference is likely to be underestimated. Unfortunately, the incompleteness of the FR0s sample prevents us from deriving a robust estimate of their jet speed.

4.2. Jet morphology

The jet morphology in many sources presented in the previous section is complex. Many FR0 jets are transversely resolved, with blobs and substructures suggesting a strong interaction with the surrounding ISM. One of the best cases is J1040+09 (Fig. 7) where at 5 GHz we see a northern jet with an S-shaped structure, and at 1.5 GHz we have a well-resolved two-sided structure. The southern one is more extended and is lobe-like extended to the east.

These features are instead not seen in the inner region of FRIs. This difference can be interpreted as being due to different jet speeds in the two classes: the slower and less energetic jets of FR0s are more affected by the presence of a nonhomogeneous external medium; the relativistic jets of FRIs are instead able to penetrate it without being deflected. Only at a distance from the jet basis of several kiloparsec, when the jet velocity decreases, do FRIs show distorted and complex morphologies.

Three FR0s, namely J1621+25, J1628+25, and J2346+00, show a Z-shaped structure. The jets are symmetric very near to the core, and move to a different PA after a few milliarcseconds at about the same distance where they form symmetric extended structures at a different PA. A similar structure has been rarely found in FRI sources and on a larger scale. The best cases are 3C 293 (van Breugel et al. 1984) and 4C 26.42 (Liuzzo et al. 2009b). These structures have been interpreted as the interaction between a low-velocity jet and a surrounding rotating gas disk structure (3C293) or as a low-velocity jet interacting with rotating accretion gas at the center of the cooling cluster A1795 (Liuzzo et al. 2009b) for 4C 26.42. This suggests that in FR0 sources the Z-shaped structure could also be due to a gas rotating disk-like structure coupled with a low-velocity jet.

We conclude that the FR0 morphology found in available VLBI images also show strong evidence that parsec-scale jets in FR0 sources are not relativistic or at most are mildly relativistic.

4.3. Missing correlated flux

We compared the correlated VLBI flux with the nuclear emission detected in JVLA images at 7.5 GHz, when available, and with other VLA images in other cases. In 40% of FR0 sources we find an agreement between the two results suggesting that VLBI images show all or most of the source nuclear structure. In a lower number (20%) we found a higher flux density in VLBI images, possibly due to source variability and/or an inverted or peculiar radio spectrum. In other sources (40%) a significant fraction of flux density is missing in VLBI images with respect to the arcsec-scale images. This loss can be due to variability, but mainly to the lack of sensitivity in VLBI images to diffuse emission; the VLBI images resolve and do not see low-brightness extended structures because of super-resolution and

spectral index effects. This is also evident when comparing high- and low-frequency VLBI images (see, e.g., the EVN images at 1.7 GHz of J1230+47 with the 8.4 GHz of the same source by Cheng & An 2018). A deep study of the sources where a significant fraction of their flux density is missing in VLBI images will allow us to understand why jets stop and die. To understand jet properties we need to understand how the jets evolve. The FR0 jets could be able to create a diffuse low-brightness lobe-like emission or an extended low-brightness jetted structure, both not visible in VLBI images. The interaction between the host galaxy and the nonthermal jet emission would be different in the two cases. Moreover, in the one-sided sources the missing flux could be due to the invisible counter-jet emission. Intermediate-scale observations (e.g., with EVN and eMERLIN) and the combination of long and short baselines (as demonstrated in Baldi et al. 2021 with eMERLIN and JVLA combined data sets) represent a powerful tool to study the missing flux, for example in a lobe-like structure created by the jet, in a longer jet becoming increasingly fainter moving far from the core, or a contribution of the counter-jet side in asymmetric sources.

4.4. Origin of the radio emission

Theoretical models indicate that an accreting SMBH is the origin of symmetric relativistic jets (see, e.g., Blandford & Königl 1979; Gomez et al. 1995 and references therein) in contrast with the low-velocity jets found here. However, observational evidence of low-velocity jets cannot exclude the presence of an inner relativistic spine surrounded by a low-velocity sheath. The main difference between FRI and FR0 jets could be the relative importance of the relativistic spine in the jet structure.

The present data are in agreement with the Garofalo & Singh (2019) model where low-power relativistic jets are expected in sources with a low prograde spinning black hole surrounded by advection dominated accretion flows. In these sources the relativistic inner spine of the jet launched by the black hole ergosphere associated with the Blandford-Znajek process (Blandford & Znajek 1977) is less prominent than that produced by the Blandford-Payne portion of the accretion disk (Blandford & Payne 1982).

In this framework we expect a jet with a subtle relativistic spine unable to extend, in most cases, to the kiloparsec scale due to instabilities. This jet is surrounded by a low-velocity sheath, which is the dominant structure visible in our images. This jet structure accounts for the nature of the very few compact FR0s, also in VLBI images (e.g., J0943+36) where the structure, the high flux density, and the high variability suggest that we are seeing a relativistic jet well aligned with the line of sight.

FR0 jets, because of the large diffuse sheath, are influenced by the ISM, but also strongly interact with it and modify its properties and physical conditions. Mapping HI on parsec scales (Murthy et al. 2022) show that a low-power jet is also able to remove cold gas from the center of a galaxy, and therefore to influence the accretion into the SMBH and the properties of the host galaxy. The large number of FR0 galaxies implies that the feedback between the energy produced by the AGN and the galaxy evolution is also present in sources where the total radio power is low because the low-velocity jet is not able to create and sustain extended radio lobes.

5. Conclusions

FR0 galaxies are the dominant local population in the radio sky. They have multiwavelength nuclear properties similar to FRI

¹ The tests were performed using a censored statistical analysis with the task twosamp within the ASURV package (Lavalley et al. 1992) implemented within the PyRAF software (Science Software Branch at STScI 2012).

radio galaxies, but show a clear deficit of extended radio structures and are largely core dominated with respect to FRI sources. Most FROs are unresolved in radio images at arcsecond resolution. For this reason VLBI observations are necessary to investigate the nature and properties of their radio emission.

From the new observations presented here and literature data we conclude the following:

1. All FRO sources observed with VLBI, with the exception of J2236+00, have been detected. This result, together with the observed jet structures visible in most VLBI images, show that the FRO radio emission is related to the nuclear activity of an accreting SMBH from where two symmetric synchrotron jets are launched.
2. The complex jet structures and the large number of two-sided structures are strong evidence that the FRO jets present in VLBI images are not relativistic, contrary to what is observed in FRI sources.
3. The properties of a few FROs also suggest the presence of a relativistic faint inner spine in these sources, as requested by the proposed identification as misoriented BL Lacs. These results are in agreement with the suggestion that FRO jets are associated with a low (and prograde) spin SMBH. In these sources jets are structured; a relativistic faint inner spine launched by the black hole ergosphere (BZ jet) is surrounded by a dominant nonrelativistic shear launched by the accretion disk (BP jet). Because of the strong interaction between the shear and the ISM, the jet cannot survive to reach the kiloparsec scale.
4. In several FRO galaxies the correlated parsec-scale flux density is a small fraction of the nuclear flux density measured at subarcsec resolution, indicating that a significant amount of radio emission is produced at intermediate scales. EVN and MERLIN observations are necessary to understand and probe this component, most likely associated with low surface brightness jets or diffuse lobes.
5. Despite the low power and small size of radio emission in FROs, our results represent clear evidence for the presence of collimated jets. This implies that AGN feedback is also at work in these sources. Recent observations have shown that a low-power jet is able to remove cold gas from the center of a galaxy, and therefore to influence the accretion onto the SMBH.

Acknowledgements. We would like to thank the Referee for useful comments. RL acknowledges financial support from the State Agency for Research of the Spanish MCIU through the “Center of Excellence Severo Ochoa” award for the Instituto de Astrofísica de Andalucía (SEV-2017-0709), from the Spanish Ministerio de Economía y Competitividad, and Ministerio de Ciencia e Innovación (grants AYA2016-80889-P, PID2019-108995GB-C21), the Consejería de Economía, Conocimiento, Empresas y Universidad of the Junta de Andalucía

(grant P18-FR-1769), the Consejo Superior de Investigaciones Científicas (grant 2019AEP112). The National Radio Astronomy Observatory is a facility of the National Science Foundation operated under cooperative agreement by Associated Universities, Inc. The European VLBI Network is a joint facility of independent European, African, Asian, and North American radio astronomy institutes.

References

- Baczko, A. K., Ros, E., Kadler, M., et al. 2022, *A&A*, **658**, A119
- Baldi, R. D., & Capetti, A. 2009, *A&A*, **508**, 603
- Baldi, R. D., & Capetti, A. 2010, *A&A*, **519**, A48
- Baldi, R. D., Capetti, A., & Giovannini, G. 2015, *A&A*, **576**, A38
- Baldi, R. D., Capetti, A., & Massaro, F. 2018, *A&A*, **609**, A1
- Baldi, R. D., Capetti, A., & Giovannini, G. 2019a, *MNRAS*, **482**, 2294
- Baldi, R. D., Torresi, E., Migliori, G., & Balmaverde, B. 2019b, *Galaxies*, **7**, 76
- Baldi, R. D., Giovannini, G., & Capetti, A. 2021, *Galaxies*, **9**, 106
- Blandford, R. D., & Königl, A. 1979, *ApJ*, **232**, 34
- Blandford, R. D., & Payne, D. G. 1982, *MNRAS*, **199**, 883
- Blandford, R. D., & Znajek, R. L. 1977, *MNRAS*, **179**, 433
- Capetti, A., Massaro, F., & Baldi, R. D. 2017, *A&A*, **598**, A49
- Capetti, A., Baldi, R. D., Brienza, M., Morganti, R., & Giovannini, G. 2019, *A&A*, **631**, A176
- Capetti, A., Brienza, M., Baldi, R. D., et al. 2020, *A&A*, **642**, A107
- Capetti, A., Brienza, M., Balmaverde, B., et al. 2022, *A&A*, **660**, A93
- Chen, Y., Gu, Q., Fan, J., et al. 2021, *ApJ*, **913**, 93
- Cheng, X. P., & An, T. 2018, *ApJ*, **863**, 155
- Cheng, X., An, T., Sohn, B. W., Hong, X., & Wang, A. 2021, *MNRAS*, **506**, 1609
- Dullo, B. T., Knapen, J. H., Williams, D. R. A., et al. 2018, *MNRAS*, **475**, 4670
- Feretti, L., Giovannini, G., Hummel, E., & Kotanyi, C. G. 1984, *A&A*, **137**, 362
- Garofalo, D., & Singh, C. B. 2019, *ApJ*, **871**, 259
- Garofalo, D., Evans, D. A., & Sambruna, R. M. 2010, *MNRAS*, **406**, 975
- Garofalo, D., Kim, M. I., Christian, D. J., et al. 2016, *ApJ*, **817**, 170
- Ghisellini, G. 2011, in American Institute of Physics Conference Series, eds. F. A. Aharonian, W. Hofmann, & F. M. Rieger, *Am. Inst. Phys. Conf. Ser.*, **1381**, 180
- Giovannini, G. 2004, *Ap&SS*, **293**, 1
- Giovannini, G., Taylor, G. B., Feretti, L., et al. 2005, *ApJ*, **618**, 635
- Gomez, J. L., Martí, J. M. A., Marscher, A. P., Ibanez, J. M. A., & Marcaide, J. M. 1995, *ApJ*, **449**, L19
- Heckman, T. M., & Best, P. N. 2014, *ARA&A*, **52**, 589
- Lavalley, M., Isobe, T., & Feigelson, E. 1992, in ASURV: Astronomy Survival Analysis Package, eds. D. M. Worrall, C. Biemesderfer, & J. Barnes, *ASP Conf. Ser.*, **25**, 245
- Liuzzo, E., Giovannini, G., Giroletti, M., & Taylor, G. B. 2009a, *A&A*, **505**, 509
- Liuzzo, E., Taylor, G. B., Giovannini, G., & Giroletti, M. 2009b, *A&A*, **501**, 933
- Liuzzo, E., Buttiglione, S., Giovannini, G., et al. 2013, *A&A*, **550**, A76
- Massaro, F., Capetti, A., Paggi, A., et al. 2020, *ApJ*, **900**, L34
- Murthy, S., Morganti, R., Wagner, A. Y., et al. 2022, *Nat. Astron.*, **6**, 488
- Panessa, F., Baldi, R. D., Laor, A., et al. 2019, *Nat. Astron.*, **3**, 387
- Sadler, E. M., Ekers, R. D., Mahony, E. K., Mauch, T., & Murphy, T. 2014, *MNRAS*, **438**, 796
- Science Software Branch at STScI 2012, Astrophysics Source Code Library [record ascl: [1207.0111](https://arxiv.org/abs/1207.0111)]
- Torresi, E., Grandi, P., Capetti, A., Baldi, R. D., & Giovannini, G. 2018, *MNRAS*, **476**, 5535
- Urry, C. M., & Padovani, P. 1995, *PASP*, **107**, 803
- van Breugel, W., Heckman, T., Butcher, H., & Miley, G. 1984, *ApJ*, **277**, 82